Applied Physics Letters ARTICLE pubs.aip.org/aip/apl

Real-time spectral interferometry enables ultrafast acoustic detection

Cite as: Appl. Phys. Lett. **123**, 211105 (2023); doi: 10.1063/5.0178453
Submitted: 27 September 2023 · Accepted: 8 November 2023 ·
Published Online: 21 November 2023

Yusong Liu,[1,2] Wenjun Ni,[3] Liuyang Yang,[1] Siyun Huang,[1] Haoguang Liu,[1] Yixiang Sun,[1] Ran Xia,[1] Yao Yao,[2] Lisong Yan,[1] Yiyang Luo,[2,a)] Zhilin Xu,[4] Gang Xu,[1] Qizhen Sun,[1] Xiahui Tang,[1] and Perry Ping Shum[5]

AFFILIATIONS

[1]School of Optical and Electronic Information, Huazhong University of Science and Technology, Wuhan 430074, China
[2]Key Laboratory of Optoelectronic Technology and Systems (Ministry of Education), Chongqing University, Chongqing 400044, China
[3]Hubei Key Laboratory of Intelligent Wireless Communications, College of Electronics and Information Engineering, South-Central Minzu University, Wuhan 430074, China
[4]Center for Gravitational Experiments, Huazhong University of Science and Technology, Wuhan 430074, China
[5]Department of Electronic and Electrical Engineering, Southern University of Science and Technology, Shenzhen 518055, China

[a)]**Author to whom correspondence should be addressed:** yyluo@cqu.edu.cn

ABSTRACT

Optical interferometry is a promising alternative for acoustic detection as it records the changes of interference patterns. Apart from interferometric sensor heads, readout systems also play a crucial role in sensing performance. Here, inspired by the soliton molecule vibrations in ultrafast lasers, we introduce an efficient real-time spectral interferometry (RSI) approach to read out the Fabry–Pérot interferometer (FPI) for acoustic detection. Broadband pulses, emitted from an ultrafast fiber laser, are launched into the FPI sensor. Pseudo dual-pulse molecule is constructed by virtue of the equivalent two-beam interference of the FPI and modulated by the diaphragm transducer. The acoustic driven "molecular vibration" conforms to the sound applied on the metal diaphragm. Hence, the acoustic signals can be directly recorded by the successive dual-pulse spectral interferograms, imaged as a spectral encoded "soundtrack." We experimentally achieve the real-time characterization of both the audible and ultra sounds by retrieving the relative phase evolutions with a phase resolution of 37.6 mrad and preliminarily verifying the feasibility of the RSI in acoustic detection. This approach to wideband acoustic detection highlights an advanced application of ultrafast laser sources and paves an efficient way for interrogating the interferometric fiber sensors.

Detection of acoustic waves ranging from infrasound signals up to ultrasound signals has attracted intensive attention, considering widespread applications in the fields of medical diagnostics, photoacoustic spectroscopy, pipeline leakage, national defense, etc.[1–8] Apart from the traditional method of piezoelectric materials, fiber optic acoustic sensors, featuring inherent advantages of compact size, corrosion resistance, and immunity to electro-magnetic interference, provide a potential alternative for wideband acoustic detection.[9–12] In particular, optical interferometry serves as a significant candidate via recording the changes of interference patterns.[13,14] Fabry–Pérot interferometer (FPI) is most frequently used because of the small-volume geometry.[15–18] Compared with the intrinsic FPI characterized by an all-fiber geometry, the diaphragm-based extrinsic one can be easily packaged as a sensing probe and allows broad response frequency band with respect to the selection of transducer materials such as polymer film, metal diaphragm, and two-dimension material film.[19,20] In this approach, the diaphragm is forced to vibrate along with the acoustic waves and then alters the interference condition by perturbating the light beams.

In the sensing system, the altered characteristics of the optical interferometry are detected and converted by the readout system.[21–24] It raised a question of how to couple the readout implementation to the optical interferometry-based acoustic detection. Typically, a narrow-linewidth continuous-wave (CW) laser is mostly employed for the sensing interrogation.[25] The operating wavelength is often tuned to the point of approximately linear region on the optical interferometric spectrum.[26] Afterward, the sound induced changes of the interference patterns would be translated into the optical intensity variations for direct detection.[27,28] However, the difficult scalability for interrogating more sensors and the susceptibility to environmental conditions

impede the practical applications of the CW-interferometry-based sensing system. Optical pulse interferometry exemplifies a more scalable and stable alternative for acoustic detection.[29] Key to this readout system is to introduce coherence-restored pulse interferometry for interrogating the interferometric acoustic sensors.[30] The broadband optical pulse is spectrally shaped by the interferometer and resonator, and then optically demodulated for detecting the spectral shifts. The sensing performance of the coherence-restored pulse interferometry is largely decoupled from the laser performance, yielding a new framework toward the optical pulse interferometry-based sensing applications.

More recently, time-stretch dispersive Fourier transform (TS-DFT), as an important key component of optical time-stretch imaging, has been implemented for revealing the ultrafast laser dynamics by mapping the spectral information onto the temporal domain.[30,31] Particularly, the real-time spectral interferometry (RSI) enables the successive recordings of multi-pulse molecular interferograms, which reminisces the acoustic detection based on optical pulse interferometry.[32–36] In this paper, drawing inspiration from these two parallel research scenarios, we introduce a real-time measurement approach of RSI into the ultrafast acoustic detection. A pulsed broadband fiber laser is employed as the sensing light source, and an extrinsic FPI is used as the sensor head. The two reflected pulses from the FPI sensor constitute a pseudo dual-pulse molecule, and the molecular vibration conforms to the acoustic signals applied on the diaphragm. The TS-DFT allows for real-time characterization of the acoustic signals via retrieving the oscillatory phase evolutions of the pseudo dual-pulse molecules with the phase resolution of 37.6 mrad. The outstanding sensing performance of the RSI approach and FPI sensor is validated for both the audible sounds and ultrasounds. This RSI-based real-time measurement offers an alternative way for the wideband acoustic detection.

To introduce the RSI into the acoustic detection, we develop a wideband acoustic detection system as shown in Fig. 1(a). A passively mode-locked fiber laser is used as the pulsed broadband sensing light source. The total length of the laser resonator is about 5.8 m, including a 1.5-m erbium-dropped fiber (EDF, Optical Fiber Cable and Connectivity Solutions, $\beta_2 = +0.061$ ps^2/m) as the gain medium and a 4.3-m single-mode fiber (SMF, $\beta_2 = -0.022$ ps^2/m). The gain medium is pumped by a 980-nm semiconductor laser diode through a hybrid wavelength division multiplexer (WDM)/isolator (ISO) module. The ISO ensures the unidirectional operation of the laser resonator. Two polarization controllers (PCs) and a polarizer implement the passive mode-locking method of nonlinear polarization rotation (NPR), which can be considered as an equivalent saturable absorber. The emitted pulses are extracted from the 10% output port of a 10:90 optical

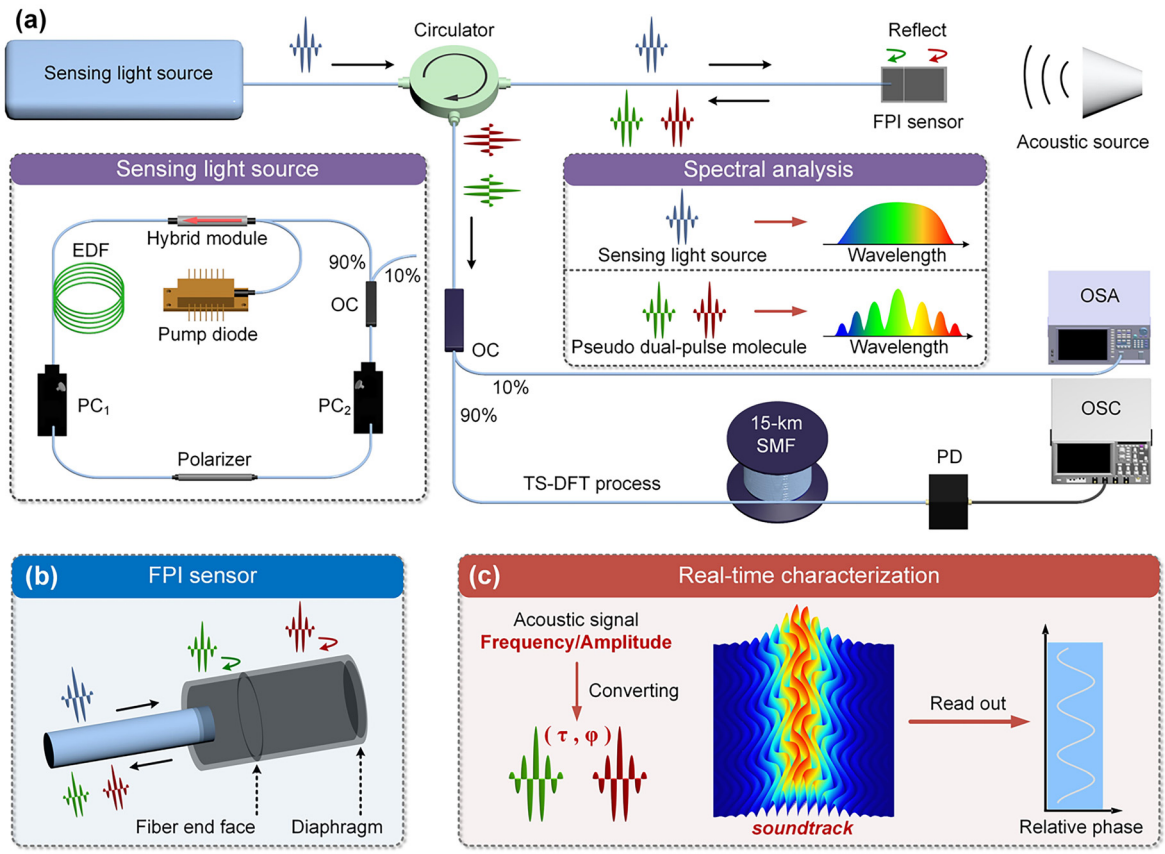

FIG. 1. (a) Configuration of the RSI-based acoustic detection system. The inset describes the pulsed sensing light source; (b) schematic diagram of the FPI sensor, illustrating the construction of the pseudo dual-pulse molecules; and (c) sketch of the real-time characterization of the acoustic signals. The acoustic information can be directly readout from the retrieved relative phase.

coupler (OC) and transmitted to the FPI sensor through a circulator. The averaged optical spectra of them are recorded by an optical spectrum analyzer (OSA, YOKOGAWA). Moreover, a 15-km SMF (SMF, $\beta_2 = -0.022$ ps^2/m) with a total dispersion of -330 ps^2 is used for the time-stretch process to realize the real-time monitoring on the spectral evolutions of the pseudo dual-pulse molecules, which are recorded by a 12-GHz photodiode (PD) and a 33-GHz oscilloscope (OSC, Agilent).

For the acoustic detection, an FPI is used as the acoustic sensor head [Fig. 1(b)]. The two reflection mirrors inside are composed of a fiber end face and an aluminum diaphragm that is in response to external acoustic stimuli. The aluminum diaphragm with a thickness of 3 μm and a reflectivity greater than 90% is used to form a $\sim$250 μm FPI cavity. Sequentially, the fiber laser is tuned to operate at single-pulse state with a center wavelength of 1560 nm and a repetition rate of 34.5 MHz. The sensing light source is input into the acoustic sensor head. Then, the two pulses that are, respectively, reflected from the fiber end face and aluminum diaphragm constitute a pseudo dual-pulse molecule with a temporal separation of a few picoseconds. In the spectral analysis, the used FPI can approximately induce an equivalent two-beam interference, leading to the spectral interferogram with a modulation period of a few nanometers. It allows for the coupling from the acoustic signal to pseudo dual-pulse molecules.

While the external stimulus reaches the sensor head, the aluminum diaphragm will experience periodic mechanical vibration, consequently resulting in the variation of the optical path difference L between these two pulses. It reminisces the molecular vibration, featuring concurrent evolutions of temporal separation $\tau = 2nL/c$ and relative phase $\varphi = 4\pi nL/\lambda$ [Fig. 1(c)].[32,33] Key to the readout system is introducing the efficient RSI to reveal the real-time spectral evolutions of the pseudo dual-pulse molecules. The evolving spectral fringe is imaged as a spectral encoded soundtrack that carries both the frequency and amplitude information of the acoustic signals. The relative phase of the acoustic driven molecular vibration would be retrieved and unwrapped by the temporal coherence function, Fourier transformed from the soundtrack. Thereout, the acoustic signals applied on the FPI sensor will be converted into the oscillatory phase evolution of the pseudo dual-pulse molecules, which enables the excellent acoustic detection based on the efficient RSI.

Herein, the optical spectra of the pulsed broadband sensing light source (probe) and the pseudo dual-pulse molecule (echo) are shown in Fig. 2(a). The free spectral range (FSR) of 4.8 nm matches the length

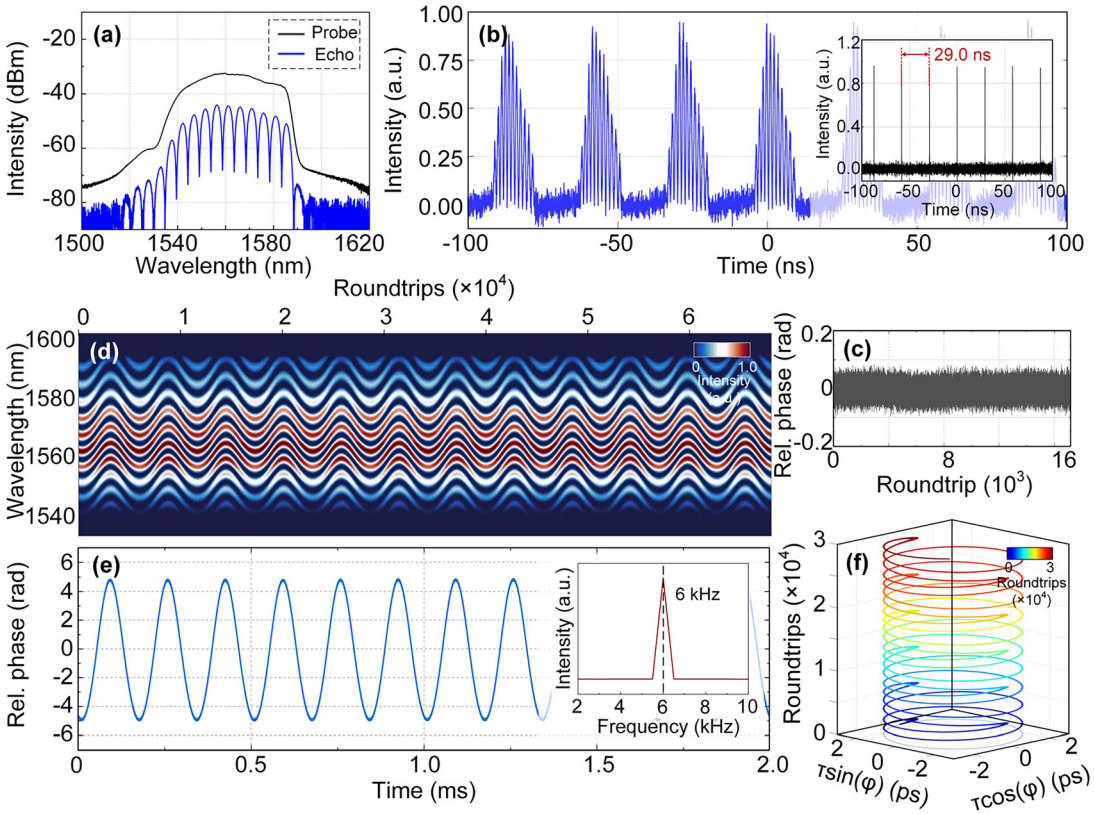

FIG. 2. Introduction on the pulsed sensing light source. (a) Averaged optical spectra of the sensing light source and the pseudo dual-pulse molecules, detected by the OSA. (b) Real-time optical spectra of the pseudo dual-pulse molecules after the TS-DFT process. The inset shows the corresponding pulse trains without the TS-DFT process. (c) Retrieved stationary relative phase without any external acoustic stimuli applied on the FPI sensor, determining the phase resolution of 37.6 mrad; exemplary 6-kHz acoustic detection. (d) Successive spectral interferograms of over 60 000 roundtrips, encoded with the 6-kHz acoustic information. (e) Retrieved oscillatory relative phase evolution, and the inset shows the oscillating frequency calculated by fast Fourier transform (FFT). (f) A 3D interaction space, visualizing the trajectory of the temporal separation and relative phase of pseudo dual-pulse molecules.

of the FPI cavity. Assisted with the TS-DFT, real-time spectral interferograms of the pseudo dual-pulse molecules are recorded [Fig. 2(b)]. To quantify the phase resolution of the phase retrieval, the stationary relative phase is exhibited in Fig. 2(c) without any external acoustic stimuli applied on the FPI sensor. The probability density function histogram of the relative phase follows the normal distribution law. Thus, we can estimate that phase resolution of this phase retrieval is about 37.6 mrad by calculating the standard deviation σ. It is equal to the diaphragm vibration amplitude of 9.37 nm, which paves an efficient way to characterize the micrometric displacement in high-precision measurements.

To exemplify the usefulness of this RSI-based acoustic detection, a continuous 6-kHz audible sound is generated from an acoustic source. The spectral encoded soundtrack is detected by recording the successive spectral interferograms of the pseudo dual-pulse molecules as shown in Fig. 2(d). The evolving spectral interferograms indicate the analogous soliton vibration dynamics. From the spectral encoded soundtrack, the relative phase φ, as a great sensitive indicator in response to external disturbances, is read out as shown in Fig. 2(e), featuring high signal-to-noise ratio (SNR). The oscillatory frequency is calculated by taking the FFT of the relative phase, which is in line with the 6-kHz acoustic signal. The frequency resolution $1/\Delta T$ is about 500 Hz, which can be improved by increasing the recorded time duration. However, the frequency accuracy f_s/N can be optimized by zero fill operation, where f_s is the sampling frequency, and N is the total data points. For better visualization, the evolving trajectory of the relative phase φ and temporal separation τ is shown in a 3D interaction space in Fig. 2(f). This 6-kHz test preliminarily demonstrates that the RSI is capable of operating real-time characterization of the acoustic signals.

Moreover, to further investigate the performance of the RSI-based acoustic detection, the intrinsic relations between the acoustic signals and the retrieved relative phases φ should be clarified. Upon increasing the acoustic pressures of the 6-kHz audible sounds, four exemplary spectral encoded soundtracks are recorded as shown in Figs. 3(a)–3(d). Obviously, in Fig. 3(e), the retrieved four relative phase evolutions indicate that the increased acoustic pressure will enhance the vibration dynamics of the pseudo dual-pulse molecules, as well as magnify the oscillatory phase amplitude. In the inset, the oscillatory amplitude increases from 5.81 to 28.28 rad. The great linear relation between the oscillatory amplitudes and the acoustic pressures ensures the fidelity of the resolved acoustic pressure. It also verifies high sensitivity of the FPI sensor and the feasibility of this RSI-based acoustic detection. We speculate that this RSI approach can be applied to detect a large range of acoustic pressure.

For certifying the frequency response of the RSI-based acoustic detection, the acoustic frequency is increased from 2 to 8 kHz but with the same amplitude [Figs. 3(f)–3(h)]. The three successive spectral

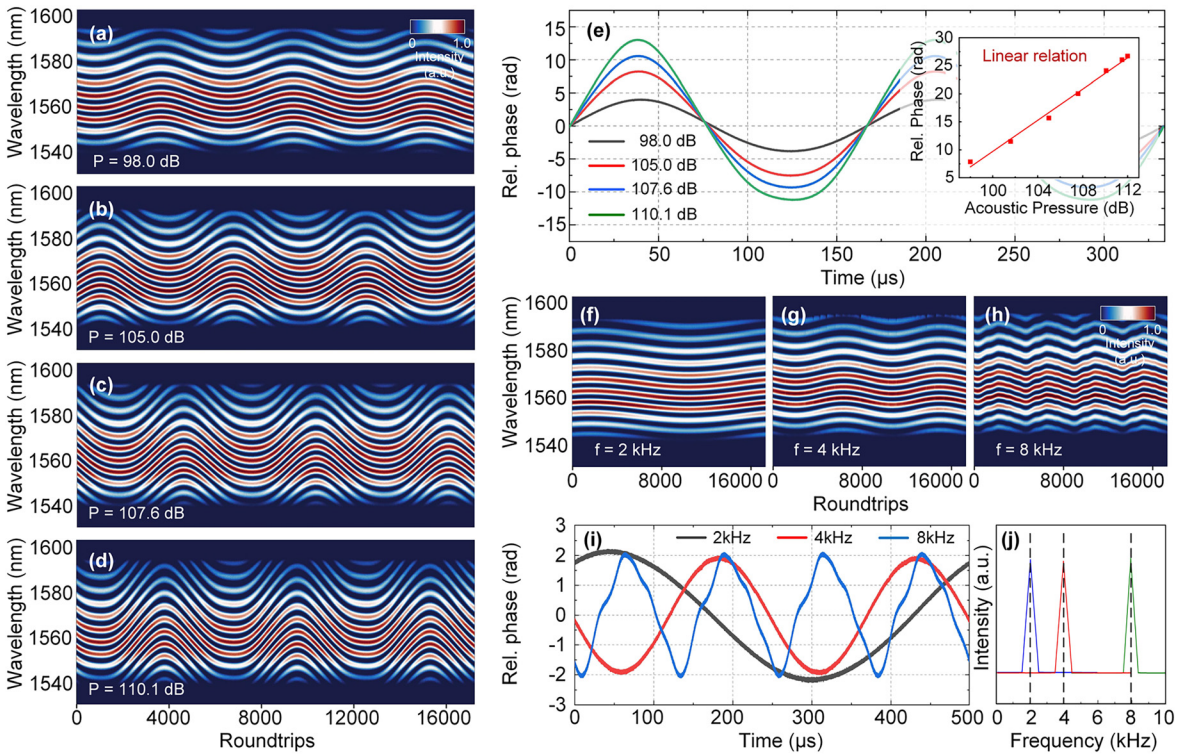

FIG. 3. Real-time characterization of audible sounds with different amplitudes and frequencies. (a)–(d) successive spectral interferograms with increased acoustic pressures from 98.0 to 110.1 dB and (e) retrieved four relative phases, characterized by different oscillatory phase amplitudes. The fitted nearly linear relation between the acoustic pressure and the oscillatory phase amplitude is exhibited in the inset. (f)–(h) Successive spectral interferograms of the audible sounds with increasing acoustic frequencies, (i) retrieved three relative phases with identical oscillatory amplitude but different frequencies, and (j) oscillatory frequencies calculated by taking FFT of the oscillatory phase evolutions.

interferograms exhibit different molecular vibrations. The related phase evolutions are read out as shown in Fig. 3(i). Notably, the oscillatory amplitudes of them are nearly identical, further verifying the great performance on measuring the acoustic pressure. These discrete frequency tests are introduced to preliminarily validate the feasibility of the RSI and the frequency response of the FPI sensor. In particular, the 8-kHz test is a little blurry. However, the calculated oscillatory frequency is still in line with the audible sounds [Fig. 3(j)]. While asking for higher-frequency acoustic detection, like ultrasounds (>20 kHz), another FPI sensor should be customized. Such real-time resolving on both the acoustic frequency and pressure validates the excellent performance of the RSI-based acoustic detection.

Beyond the simplex-frequency acoustic detection, real-time characterization of audible sounds in complicated multi-frequency scenarios is also a considerable challenge. Herein, different multi-frequency-mixed audible sounds are generated to further test the performance of the RSI-based acoustic detection in complicated scenarios. These mixed acoustic signals applied on the metal diaphragm of the FPI sensor will induce composite mechanical vibrations. Accordingly, the spectral encoded soundtracks of the two scenarios are recorded and resolved as shown in Fig. 4. The calculated multiple oscillatory frequencies agree well with the mixed audible sounds. We can briefly summarize that this real-time measurement can not only realize the precise retrieval of wideband acoustic signals but also be applied to complicated multi-frequency scenarios, consequently providing an excellent perspective for interrogating the interferometric fiber sensors.

Inspired by the high-speed response of the RSI approach, we have made further investigation of its feasibility in higher-frequency scenarios of ultrasounds (>20 kHz). The sensing light source is upgraded by increasing the pulse repetition rate to 54.86 MHz for higher frequency accuracy. In the meantime, another sensor head centering at 100 kHz is developed. Similarly, it is also made of a fiber end face and an aluminum diaphragm with a reflectivity of over 90%. In this paragraph, the sensor head and an ultrasound source are closely placed under water [Fig. 5(a)]. The optical spectrum of the pseudo dual-pulse molecule with an FSR of 4.6 nm is shown in Fig. 5(b), in line with the length of the FPI cavity of 260 μm. To test the performance of the FPI sensor, the acoustic frequency of the ultrasound is increased from 20 to 200 kHz, with a step of 10 kHz. The exemplary 30 and 100-kHz measurements portraying different molecular vibrations are shown in Figs. 5(c) and 5(d), embedded with the retrieved oscillatory phase evolutions. Likewise, the phase resolution of this sensing light source can be evaluated about 41.7 mrad, a little different from the light source used for audible sounds. The calculated oscillatory frequencies agree well with the acoustic frequencies, verifying the excellent frequency response of the FPI sensor [Fig. 5(e)]. Thus, the efficient RSI can perform well in both the audible sounds and ultrasounds, preliminarily validating the feasibility of this real-time measurement in wideband acoustic detections.

To further test the performance of the RSI-based acoustic detection in complicated scenarios, the dual-frequency ultrasounds of 60 and 80 kHz, and 80 and 120 kHz are generated as the under-test signals. The mixed ultrasounds applied on the aluminum diaphragm of the sensor head are read out as shown in Figs. 5(f) and 5(g). The calculated oscillatory phase frequencies are in line with the acoustic frequencies. Therefore, the RSI and FPI sensors are certified with great performance in acoustic detections, further verifying the feasibility of this real-time measurement. It can be speculated that the efficient RSI might have potential in more complicated scenarios, like the ultrasounds with certain bandwidths. While asking for better frequency resolution of the acoustic detection, the pulsed light source should be upgraded by increasing recorded time duration or the zero fill operation. Better phase resolution requires further upgradation of the parameter setting of the entire system, such as the stability of the light

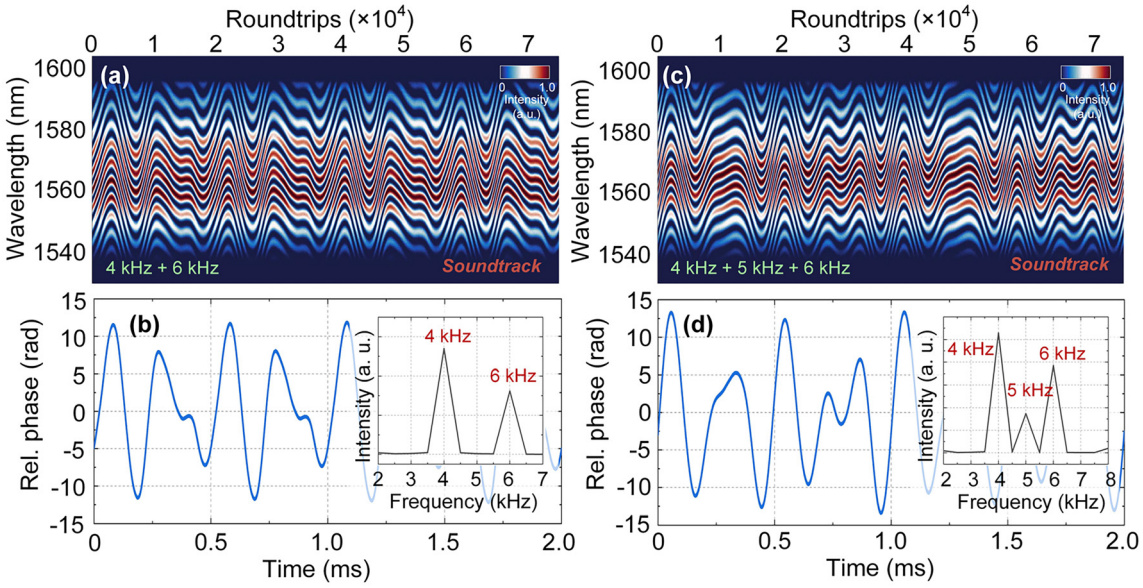

FIG. 4. Exemplary multi-frequency tests of audible sounds. (a) Successive spectral interferograms of the two-frequency-mixed audible sound; (b) retrieved relative phase, and the inset describes the two oscillatory frequencies (4, 6 kHz) calculated by FFT; (c) successive spectral interferograms of the three-frequency-mixed audible sound; and (d) retrieved relative phase, and the inset describes the three oscillatory frequencies (4, 5, 6 kHz) calculated by FFT.

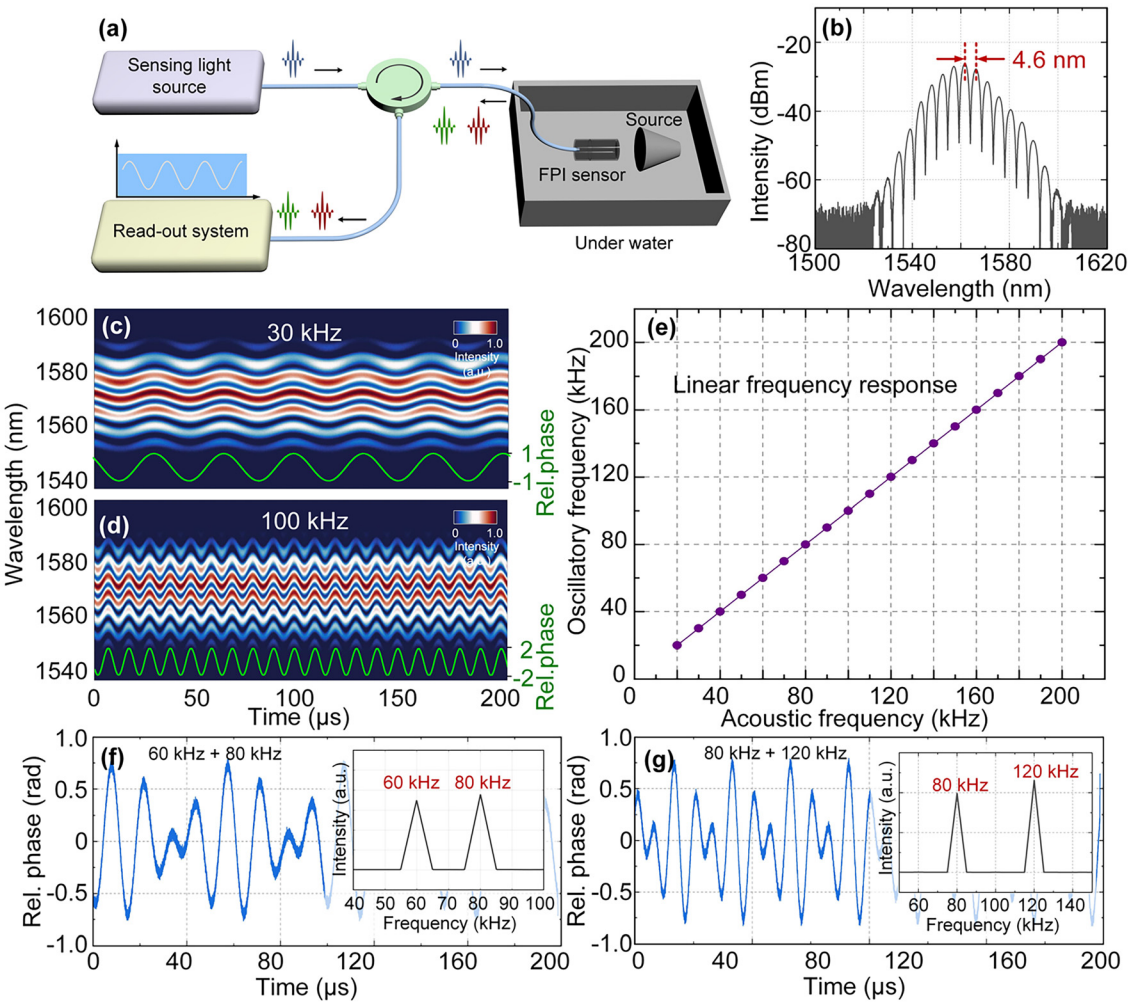

FIG. 5. Acoustic detection for ultrasounds with different frequencies. (a) System configuration of the real-time detection for ultrasounds. Particularly, the ultrasound source and the upgraded FPI sensor are closely placed under water; (b) optical spectrum of the pseudo dual-pulse molecules; (c) and (d) exemplary successive spectral interferograms of 30 and 100 kHz ultrasounds; (e) great linear relation between the oscillatory frequencies and the under-test ultrasounds, from 20 kHz to 200 kHz, indicating the excellent frequency response; and (f) and (g) retrieved oscillatory relative phases of the mixed ultrasounds of 60 and 80 kHz, and 80 and 120 kHz. The insets depict the oscillatory frequencies calculated by FFT.

source, the bandwidth of the detectors, the spectral resolution of the real-time spectra, etc. This efficient RSI approach is mostly used together with the pulsed sensing light source to characterize the real-time evolutions of the spectral interferograms of pseudo dual-pulse molecules. It can be considered as a high-performance indirect measurement in acoustic detection, also having potential to detect high-frequency micro vibrations. In particular, apart from the precise retrieval of acoustic frequency or amplitude, the RSI can be also applied to realize the spatial location of a pulsed ultrasound source. Its precise location can be obtained by calculating the time delays from the ultrasound pulse source to an FPI sensor array, and we are working on it.

In conclusion, we introduce the efficient RSI to realize the real-time characterization of wideband acoustic signals, providing an excellent perspective for interrogating the interferometric fiber sensors. A broadband pulsed sensing light source is employed to carry the spectral encoded soundtrack. The acoustic frequency and pressure information are transferred into the oscillatory phase evolutions of pseudo dual-pulse molecules. Compared to existing resolving methods, the phase retrieval strategy with the phase resolution of 37.6 mrad greatly simplifies the readout process and maintains high SNR in the meantime. The great linear relation between the acoustic pressure and oscillatory amplitude ensures the fidelity when detecting a large range of acoustic pressure. It also verifies high sensitivity of the FPI sensor and the feasibility of this RSI-based acoustic detection. The quantitative discussion provides sufficient support to verify the feasibility of the efficient RSI and FPI sensor. All these results highlight the high performance of the RSI approach and FPI sensor in wideband acoustic detection, further fueling the advanced applications of ultrafast laser sources and sensing techniques.

This work was supported by the National Natural Science Foundation of China (Nos. U22A20206, 61922033, and 62275097), the Open Project Program of Wuhan National Laboratory for Optoelectronics (No. 2022WNLOKF007), the China Postdoctoral Science Foundation (No. 2022M711243), and the Fundamental Research Funds for the Central Universities (No. 2023CDJXY-041).

AUTHOR DECLARATIONS

Conflict of Interest

The authors have no conflicts to disclose.

Author Contributions

Yusong Liu: Conceptualization (lead); Data curation (lead); Investigation (lead); Writing – original draft (lead). **Yiyang Luo:** Conceptualization (equal); Project administration (equal); Supervision (equal); Writing – review & editing (equal). **Zhilin Xu:** Methodology (equal); Writing – review & editing (equal). **Gang Xu:** Methodology (equal). **Qizhen Sun:** Project administration (equal); Supervision (equal). **Xiahui Tang:** Supervision (equal). **Perry Ping Shum:** Supervision (equal). **Wenjun Ni:** Conceptualization (equal); Investigation (equal); Methodology (equal). **Liuyang Yang:** Investigation (equal). **Siyun Huang:** Data curation (equal); Investigation (equal). **Haoguang Liu:** Investigation (equal). **Yixiang Sun:** Investigation (equal). **Ran Xia:** Conceptualization (equal); Investigation (equal). **Yao Yao:** Investigation (equal). **Lisong Yan:** Methodology (equal).

DATA AVAILABILITY

The data that support the findings of this study are available from the corresponding author upon reasonable request.

REFERENCES

[1]W. Yan, G. Noel, G. Loke, E. Meiklejohn, T. Khudiyev, J. Marion, G. Rui, J. Lin, J. Cherston, A. Sahasrabudhe, J. Wilbert, I. Wicaksono, R. W. Hoyt, A. Missakian, L. Zhu, C. Ma, J. Joannopoulos, and Y. Fink, Nature **603**, 616–623 (2022).
[2]J. A. Guggenheim, J. Li, T. J. Allen, R. J. Colchester, S. Noimark, O. Ogunlade, I. P. Parkin, I. Papakonstantinou, A. E. Desjardins, E. Z. Zhang, and P. C. Beard, Nat. Photonics **11**, 714–719 (2017).
[3]Y. Liang, H. Sun, L. Cheng, L. Jin, and B. Guan, Nat. Commun. **12**, 4139 (2021).
[4]C. Lang, J. Fang, H. Shao, X. Ding, and T. Lin, Nat. Commun. **7**, 11108 (2016).
[5]H. Tang, P. Psota, J. J. Rosowski, C. Furlong, and J. T. Cheng, Light: Adv. Manuf. **3**(2), 1 (2022).
[6]C. Li and L. V. Wang, Phys. Med. Biol. **54**(19), R59–R97 (2009).
[7]X. Wang, Y. Pang, G. Ku, X. Xie, G. Stoica, and L. V. Wang, Nat. Biotechnol. **21**, 803–806 (2003).
[8]P. Beard, Interface Focus **1**(4), 602–631 (2011).
[9]L. Yang, Y. Li, F. Fang, L. Li, Z. Yan, L. Zhang, and Q. Sun, Opto-Electron. Adv. **5**(6), 200076 (2022).
[10]B. Sarkar, D. K. Mishra, C. Koley, N. K. Roy, and P. Biswas, IEEE Sens. J. **16**(22), 7950–7957 (2016).
[11]A. Hekmati and R. Hekmati, IET Sci., Meas. Technol. **11**(5), 581–589 (2017).
[12]Y. Qiu, J. Gigliotti, M. Wallace, F. Griggio, C. Demore, S. Cochran, and S. Trolier-Mckinstry, Sensors **15**(4), 8020–8041 (2015).
[13]Y. Tong, X. Guo, M. Li, H. Tang, N. Sharmin, Y. Xu, W. N. Lee, K. K. Tsia, and K. K. Y. Wong, Adv. Photonics Nexus **2**(1), 016002 (2022).
[14]D. Claus, I. Alekseenko, M. Grabherr, G. Pedrini, and R. Hibst, Light: Adv. Manuf. **2**(4), 29 (2021).
[15]H. Fan, L. Zhang, S. Gao, L. Chen, and X. Bao, Opt. Lett. **44**(15), 3606–3609 (2019).
[16]X. Wang, Y. Jiang, Z. Li, W. Wang, and Z. Li, J. Lightwave Technol. **37**(17), 4229–4235 (2019).
[17]Z. Zhang, J. He, B. Du, F. Zhang, and Y. Wang, Opt. Lett. **43**(24), 6009–6012 (2018).
[18]X. Zhang, H. Pan, H. Bai, M. Yan, J. Wang, C. Deng, and T. Wang, Opt. Lett. **43**(10), 2268–2271 (2018).
[19]W. Ni, P. Lu, X. Fu, W. Zhang, P. P. Shum, H. Sun, C. Yang, D. Liu, and J. Zhang, Opt. Express **26**(16), 20758 (2018).
[20]J. Bauer-Marschallinger, K. Felbermayer, and T. Berer, Biomed. Opt. Express **8**(9), 3938–3951 (2017).
[21]J. N. Dash, Z. Liu, D. S. Gunawardena, and H. Y. Tam, Opt. Lett. **44**(14), 3546–3549 (2019).
[22]Y. Wang, Q. Huang, W. Zhu, and M. Yang, IEEE Photonics Technol. Lett. **30**(9), 833–836 (2018).
[23]Z. Wu, H. Zhang, P. P. Shum, X. Shao, T. Huang, Y. M. Seow, Y. Liu, H. Wei, and Z. Wang, Opt. Express **23**(26), 33001–33007 (2015).
[24]S. Basiri-Esfahani, C. R. Myers, A. Armin, J. Combes, and G. J. Milburn, Opt. Express **23**(12), 16008–16023 (2015).
[25]L. Yang, C. Dai, A. Wang, G. Chen, D. Xu, Y. Li, Z. Yan, and Q. Sun, Opt. Lett. **47**(15), 3700–3703 (2022).
[26]B. Chen, Y. Chen, and C. Ma, Biomed. Opt. Express **11**(5), 2607–2618 (2020).
[27]R. Ansari, E. Z. Zhang, A. E. Desjardins, and P. C. Beard, Light: Sci. Appl. **7**, 75 (2018).
[28]G. Li, Z. Guo, and S.-L. Chen, Opt. Express **25**(21), 25023–25035 (2017).
[29]K. Goda, A. Mahjoubfar, C. Wang, A. Fard, J. Adam, D. R. Gossett, A. Ayazi, E. Sollier, O. Malik, E. Chen, Y. Liu, R. Brown, N. Sarkhosh, D. Di Carlo, and B. Jalali, Sci. Rep. **2**, 445 (2012).
[30]A. Rosenthal, S. Kellnberger, D. Bozhko, A. Chekkoury, M. Omar, D. Razansky, and V. Ntziachristos, Laser Photonics Rev. **8**(3), 450–457 (2014).
[31]C. Lei, B. Guo, Z. Cheng, and K. Goda, Appl. Phys. Rev. **3**(1), 011102 (2016).
[32]G. Herink, F. Kurtz, B. Jalali, D. R. Solli, and C. Ropers, Science **356**, 50–54 (2017).
[33]Z. Q. Wang, K. Nithyanandan, A. Coillet, P. Tchofo-Dinda, and P. Grelu, Nat. Commun. **10**, 830 (2019).
[34]Y. Liu, S. Huang, Z. Li, H. Liu, Y. Sun, R. Xia, L. Yan, Y. Luo, H. Liu, G. Xu, Q. Sun, X. Tang, and P. P. Shum, Light: Sci. Appl. **12**, 123 (2023).
[35]Y. Luo, R. Xia, P. P. Shum, W. Ni, Y. Liu, H. Q. Lam, Q. Sun, X. Tang, and L. Zhao, Photonics Res. **8**(6), 884–891 (2020).
[36]S. Huang, Y. Liu, H. Liu, Y. Sun, R. Xia, W. Ni, Y. Luo, L. Yan, H. Liu, Q. Sun, P. P. Shum, and X. Tang, APL Photonics **8**(3), 036105 (2023).